SIGNAL PROCESSING ALGORITHMS FOR REMOVING BANDING ARTIFACTS IN MRI

Marcus Björk[a], Erik Gudmundson[b,c], Joëlle K. Barral[d], and Petre Stoica[a]

[a]Department of Information Technology, Systems and Control, Uppsala University, Uppsala, Sweden
[b]Centre for Mathematical Sciences, Lund University, Lund, Sweden
[c]Signal Processing Lab, ACCESS Linnaeus Center, KTH - Royal Institute of Technology, Sweden
[d]Department of Bioengineering, Stanford University, Stanford, USA
Email: marcus.bjork@it.uu.se, erikg@maths.lth.se, jbarral@mrsrl.stanford.edu, ps@it.uu.se

ABSTRACT

In magnetic resonance imaging (MRI), the balanced steady-state free precession (bSSFP) pulse sequence has shown to be of great interest, due to its relatively high signal-to-noise ratio in a short scan time. However, images acquired with this pulse sequence suffer from banding artifacts due to off-resonance effects. These artifacts typically appear as black bands covering parts of the image and they severely degrade the image quality. In this paper, we present a fast two-step algorithm for estimating the unknowns in the signal model and removing the banding artifacts. The first step consists of rewriting the model in such a way that it becomes linear in the unknowns (this step is named Linearization for Off-Resonance Estimation, or LORE). In the second step, we use a Gauss-Newton iterative optimization with the parameters obtained by LORE as initial guesses. We name the full algorithm LORE-GN. Using both simulated and *in vivo* data, we show the performance gain associated with using LORE-GN as compared to general methods commonly employed in similar cases.

1. INTRODUCTION

Magnetic resonance imaging (MRI) is a powerful imaging technique primarily used in medical settings as a non-invasive tool for the examination of internal structures. Since the introduction of the technique in the 1970's, a large number of acquisition protocols have been proposed. One of the greatest challenges of MRI is to acquire an image with a high signal-to-noise ratio (SNR) in a short scan time, and for this, the balanced steady-state free precession (bSSFP) sequence has proven to be of great interest. A detailed explanation of bSSFP is beyond the scope of this paper, and the reader is referred to, e.g., [1, 2]. The main drawback of bSSFP is due to off-resonance effects, typically manifesting as banding artifacts [3]. These are a major concern, especially when using high field strengths. Off-resonance effects can lead to signal losses in parts of the image and techniques for improving the image quality are necessary.

Acquiring images with different phase increments, also called *phase cycling*, and combining them allows for a removal of the off-resonances. Several techniques have been proposed, for example *sum-of-squares* (SoS), where the square root of the sum of the squared magnitude of the images is used; or *maximum-intensity* (MI), where the final image is constructed by assigning to each pixel the largest magnitude of the corresponding pixel in all images. See [3] and the references therein for a more detailed explanation of the methods. These simple methods have proven useful for mitigating banding artifacts but can sometime give poor results; additionally they do not give estimates of the model parameters, which can be of great interest in quantitative MRI. Recently, attempts to remove the banding artifacts with the use of a signal model have been made. In [4], the authors used the special case occurring when setting the echo time, TE, to zero and acquiring data with a specific choice of phase increments. Then, the off-resonance effects can be removed using an analytical solution. However, this approach appears to be sensitive to noise and still does not provide estimates of all unknown parameters in the model equation. Furthermore, the method cannot be generalized to more than four phase-cycled images. In [5], the authors proposed to identify some of the unknown model parameters while fixing the others and using a standard Levenberg-Marquardt (LM) nonlinear minimization algorithm with manual initialization for the parameter estimation. This method 1) uses magnitude data, which makes the estimation less tractable from a mathematical viewpoint; 2) changes the noise properties from a Gaussian distribution to a Rician distribution, making the nonlinear least squares (NLS) criterion suboptimal (i.e., biased); and 3) causes a phase ambiguity, making it difficult to determine the off-resonance frequency. Additionally, this approach requires prior knowledge regarding the unknown parameters, and since these can vary significantly over an image, the estimated parameters are not always reliable.

In this paper, we instead propose an algorithm that has no limitations in the choice of the echo time, TE, nor the repetition time, TR, and which does not demand prior assumptions on any of the variables. Moreover, it does not need a manual initialization but rather uses a pixel-wise adaptive automatic initialization. Using complex data, all unknown parameters in the model equation are identified unambiguously, based on a model derived from [1].

2. SIGNAL MODEL

In bSSFP imaging, the complex signal, S, at an arbitrary pixel of the n^{th} image, can be modeled as [1, 2]

$$S_n = KMe^{-\frac{TE}{T_2}} e^{i(\Omega+\Delta\Omega_n)TE} \frac{1-ae^{-i(\Omega+\Delta\Omega_n)TR}}{1-b\cos\left[(\Omega+\Delta\Omega_n)TR\right]} + v_n, \tag{1}$$

where $\Omega = 2\pi f_{OR}$ with f_{OR} being the unknown off-resonance frequency, $\Delta\Omega_n$ is the user-controlled phase increment, M is the magnetization, $K \in \mathbb{C}$ is the coil sensitivity, and v_n denotes the noise, which is assumed to be independent and

complex Gaussian distributed. In this article, data was acquired by changing the centre frequency, which mimics phase cycling but adds a $\Delta\Omega_n$ in the first exponential term of (1). Furthermore,

$$M = iM_0 \frac{(1-E_1)\sin\alpha}{1-E_1\cos\alpha-(E_1-\cos\alpha)E_2^2}, \tag{2}$$

$$a = E_2, \tag{3}$$

$$b = E_2 \frac{1-E_1\cos\alpha-E_1+\cos\alpha}{1-E_1\cos\alpha-(E_1-\cos\alpha)E_2^2}, \tag{4}$$

where $E_1 = e^{-TR/T_1}$, $E_2 = e^{-TR/T_2}$, M_0 is the unknown equilibrium magnetization, and α is the tip angle (which will be considered known). T_1 is the spin-lattice relaxation time and T_2 the spin-spin relaxation time. It can be shown that $a \in [0,1]$ and $b \in [0,1]$ due to the physical constraint that all times are positive. To simplify the notation we introduce the following variables: $S_0 = KMe^{-TE/T_2}$, $\theta = \Omega TR$, $\Delta\theta_n = \Delta\Omega_n TR$ and $\theta_n = \theta + \Delta\theta_n$. The general model in (1) can then be rewritten as

$$S_n = S_0 e^{i\theta_n TE/TR}\frac{1-ae^{-i\theta_n}}{1-b\cos(\theta_n)} + v_n = g_n(\mathbf{u}) + v_n, \tag{5}$$

where $g_n(\mathbf{u})$ is the noise-free data and $\mathbf{u}$ the vector of model parameters. Acquiring images with different phase increments $\Delta\theta_n$ allows us to estimate the unknown model parameters $S_0 \in \mathbb{C}$, $a, b, \theta \in \mathbb{R}$ of (5). Even though no assumptions are made on the increments, using four images ($N = 4$) with phase shifts $\Delta\theta = [0, \pi/2, \pi, 3\pi/2]^T$ is common practice and will therefore be considered here as well. Time limits the number of images that can be acquired in practice.

3. THE LORE-GN ALGORITHM

In order to estimate the unknown parameters and remove the off-resonance (f_{OR}), we propose a two-step algorithm. The first step is named Linearization for Off-Resonance Estimation (LORE). The second step is a Gauss-Newton search (GN), hence we name the full algorithm LORE-GN. We first rewrite the model in (5) so that it becomes linear in the unknown parameters, by making use of an over-parameterization. This enables the application of ordinary least squares (LS) for obtaining an initial estimate. In the following step, the final estimates are obtained using a Gauss-Newton iterative search, using the LORE estimate as an initial guess. This step is used for fine tuning and removing bias due to errors in variables.

3.1 Step 1: Initial Estimation Using LORE

For the LORE algorithm, we introduce the following complex parameters:

$$\tilde{S}_n = S_n e^{-i\Delta\theta_n TE/TR}, \tag{6}$$

$$\alpha = S_0 e^{i\theta TE/TR}, \tag{7}$$

$$\beta = S_0 a e^{i\theta(TE/TR-1)}, \tag{8}$$

$$\gamma = be^{i\theta}, \tag{9}$$

where $\tilde{S}_n$ is known. This enables us to rewrite the noise-free part of (5) as

$$\tilde{S}_n = \frac{\alpha - \beta e^{-i\Delta\theta_n}}{1-\mathfrak{Re}(\gamma e^{i\Delta\theta_n})}, \tag{10}$$

where $\mathfrak{Re}(z)$ denotes the real part of z; similarly $\mathfrak{Im}(z)$ denotes the imaginary part. Note that if true phase cycling were used instead of changing the centre frequency, we have $\tilde{S}_n = S_n$. To simplify the notation we let $x_r = \mathfrak{Re}(x)$ and $x_i = \mathfrak{Im}(x)$. We can now express (10) in linear form:

$$\tilde{S}_n[1-\gamma_r\cos\Delta\theta_n - \gamma_i\sin\Delta\theta_n)] = \alpha - \beta e^{-i\Delta\theta_n}. \tag{11}$$

By moving the unknown variables to the right hand side and gathering the real and imaginary parts of $\tilde{S}_n$ separately in a vector as $\mathbf{y}_n = \begin{bmatrix}\tilde{S}_{r,n} & \tilde{S}_{i,n}\end{bmatrix}^T$, we can write (11) in matrix form as

$$\mathbf{y}_n = \underbrace{\begin{bmatrix} 1 & 0 \\ 0 & 1 \\ -\cos(\Delta\theta_n) & \sin(\Delta\theta_n) \\ -\sin(\Delta\theta_n) & -\cos(\Delta\theta_n) \\ \tilde{S}_{r,n}\cos(\Delta\theta_n) & \tilde{S}_{i,n}\cos(\Delta\theta_n) \\ -\tilde{S}_{r,n}\sin(\Delta\theta_n) & -\tilde{S}_{i,n}\sin(\Delta\theta_n) \end{bmatrix}^T}_{\mathbf{A}_n} \underbrace{\begin{bmatrix}\alpha_r \\ \alpha_i \\ \beta_r \\ \beta_i \\ \gamma_r \\ \gamma_i\end{bmatrix}}_{\mathbf{x}}. \tag{12}$$

Note the slight over-parameterization with six parameters as opposed to five real-valued parameters in (5). By stacking the measurements in a vector $\mathbf{y} = [\mathbf{y}_1 \cdots \mathbf{y}_N]^T$ and a matrix $\mathbf{A} = \begin{bmatrix}\mathbf{A}_1^T \cdots \mathbf{A}_N^T\end{bmatrix}^T$, where N is the number of images, we obtain $\mathbf{y} = \mathbf{A}\mathbf{x}$, from which the LS estimate of $\mathbf{x}$ is readily found as (see, e.g., [6]):

$$\hat{\mathbf{x}} = (\mathbf{A}^T\mathbf{A})^{-1}\mathbf{A}^T\mathbf{y}. \tag{13}$$

Estimates of the sought parameters can then be obtained as

$$\hat{\theta} = -\angle\left(\hat{\beta}/\hat{\alpha}\right), \tag{14}$$

$$\hat{a} = |\hat{\beta}/\hat{\alpha}|, \tag{15}$$

$$\hat{b} = |\hat{\gamma}|, \tag{16}$$

$$\hat{S}_0 = \hat{\alpha}e^{-i\hat{\theta}TE/TR}. \tag{17}$$

The information in γ regarding the off-resonance is not used since γ is usually small in magnitude, leading to unreliable estimates. We note that since the measurement noise will also enter the regressor matrix $\mathbf{A}$, these estimates will in general be biased. However, the estimates can be used as a reasonably accurate initial guess for the next step.

3.2 Step 2: Fine Tuning Using Gauss-Newton

Since the estimates obtained from LORE are biased, we propose to use a Gauss-Newton (GN) iterative method to minimize the NLS and further improve the results. GN is chosen since it is simple, computationally efficient and has fast convergence [7]. The minimization method is, however, unconstrained, so the physical constraints on a and b cannot be taken into account. What distinguishes this method from other general methods is that given a good initial estimate, here provided by LORE, GN converges to the correct optimum with high probability. If the stability of GN is compromised as a result of poor initial estimates, constrained optimization algorithms are preferable; however, they are generally more time consuming. Due to the known periodic behavior of the model, some of the non-physical local minima

can be removed by post-processing. The following relation holds:

$$S_0 e^{i\theta_n TE/TR}\frac{1-ae^{-i\theta_n}}{1-b\cos(\theta_n)} = S_0 e^{\mp i\pi TE/TR} e^{i(\theta_n \pm \pi)TE/TR}\frac{1+ae^{-i(\theta_n\pm\pi)}}{1+b\cos(\theta_n\pm\pi)}, \quad (18)$$

therefore there will be a global optimum at negative a and b corresponding to a shifted θ and rotated S_0. This fact is used in both the custom GN algorithm and the unconstrained LM algorithm. However, if the parameter b is small, there is always some risk, even at high SNR, that the global minimum occurs at a and b with different signs, and this cannot be resolved by (18).

The NLS criterion is:

$$L(\mathbf{u}) = \sum_{n=1}^{N} |S_n - g_n(\mathbf{u})|^2. \quad (19)$$

Letting $\mathbf{r}$ denote the residual vectorized over the measurements, according to

$$\mathbf{r} = \begin{bmatrix}\Re\mathfrak{e}(\mathbf{S})\\ \Im\mathfrak{m}(\mathbf{S})\end{bmatrix} - \begin{bmatrix}\Re\mathfrak{e}(\mathbf{g}(\mathbf{u}))\\ \Im\mathfrak{m}(\mathbf{g}(\mathbf{u}))\end{bmatrix}, \quad (20)$$

the update formula for GN is

$$\mathbf{u}_{k+1} = \mathbf{u}_k + c(\mathbf{J}_k^T\mathbf{J}_k)^{-1}\mathbf{J}_k^T\mathbf{r}_k, \quad (21)$$

where $\mathbf{J}_k$ is the Jacobian matrix of the vectorized model $\mathbf{g}(\mathbf{u})$ at the current point in the parameter space $\mathbf{u}_k$. The step length c is chosen by back-tracking so that the *Armijo condition* is fulfilled, that is, $c = 2^{-m}$, where m is the smallest nonnegative integer that fulfills

$$L(\mathbf{u}_{k+1}) \leq L(\mathbf{u}_k) - \mu c\mathbf{r}_k^T\mathbf{J}_k(\mathbf{J}_k^T\mathbf{J}_k)^{-1}\mathbf{J}_k^T\mathbf{r}_k, \quad (22)$$

where $\mu \in [0,\ 1]$ is a constant used to enforce a certain decrease in the criterion [8]. A stopping condition based on the norm of the gradient $\|\mathbf{J}_k^T\mathbf{r}_k\|$ and a fixed tolerance were used.

4. NUMERICAL RESULTS

4.1 Simulations

Monte Carlo simulations were performed in MATLAB, giving the root mean square error (rMSE) of the parameter estimates. The performance of the proposed algorithm was compared to 1) an unconstrained Levenberg-Marquardt algorithm (LM) as suggested by Santini *et al.* [5] in a similar case, and 2) a constrained version of LM (cLM) imposing $a \in [0,\ 1]$ and $b \in [0,\ 1]$, suggested by us as an improvement of the method in [5]. The estimates obtained with LORE were also included to illustrate the accuracy of the initial estimates, along with the optimum performance given by the Cramér-Rao lower bound (CRB), see appendix A. The standard MATLAB LM implementation in the function "lsqnonlin" was utilized. The rMSE is defined as:

$$rMSE(\hat{z}) = \sqrt{\frac{1}{M}\sum_{m=1}^{M}|\hat{z}_m - z|^2} \quad (23)$$

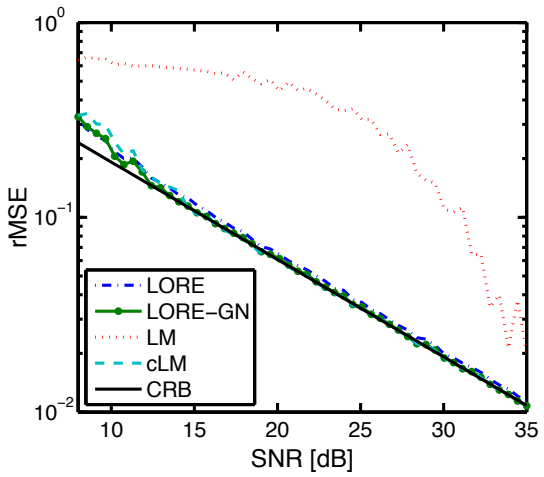

Figure 1: rMSE of the estimate $\hat{S}_0$ vs. SNR for the different methods and compared to the CRB.

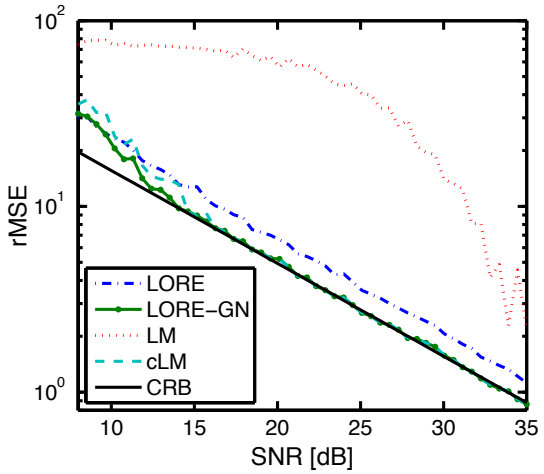

Figure 2: rMSE of the estimate $\hat{\theta}$ vs. SNR for the different methods and compared to the CRB.

where $\hat{z}_m$ is the parameter estimate of simulation m and M is the number of simulations. The parameters used in the simulations were $TR = 31.2$ ms, $TE = 15.6$ ms, $T_1 = 500$ ms, $T_2 = 50$ ms, and $\alpha = 90°$, which corresponds to the model parameters $a = 0.536$ and $b = 0.0444$. The remaining parameters were chosen as $S_0 = e^{i\pi/4}$ and $\theta = 90°$. The start values for LM and cLM were set by assuming approximate knowledge of the T_1 and T_2 parameters, since this would be true in a non-simulated case. Unfortunately, there is no available *a priori* knowledge on θ or S_0, so θ is set to zero and S_0 is chosen as the complex value of the maximum intensity sample (pixel). The initial values in the simulations were $\tilde{a} = 0.660$, $\tilde{b} = 0.0461$, $\tilde{S}_0 = 1.009 - 1.064i$ and $\tilde{\theta} = 0°$. This simulated case is in many ways simpler than the *in vivo* case. For example, here the guess has a constant offset from the true parameter values for all Monte Carlo simulations. To give a reliable average, 1000 simulations were performed at each SNR. The data was generated by adding complex noise

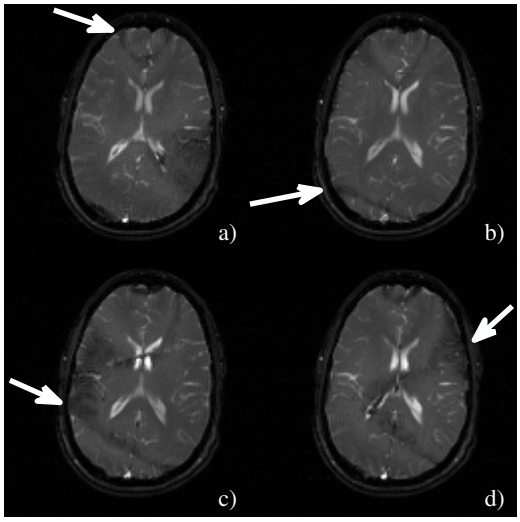

Figure 3: Magnitude images of the data showing banding artifacts due to off-resonance effects (indicated by the arrows). a), b), c) and d) correspond to images acquired at the phase shifts $\Delta\theta = 0,\ \pi/2,\ \pi$ and $3\pi/2$, respectively.

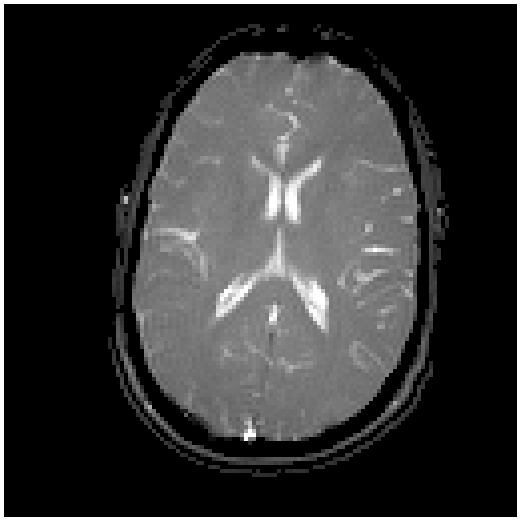

Figure 4: Estimate of $\hat{S}_0$, obtained from the proposed LORE-GN method, showing no visible banding artifacts.

of appropriate variance σ^2 according to:

$$SNR = \frac{\sum_{n=1}^{N} |g_n(\mathbf{u})|^2}{N\sigma^2}, \tag{24}$$

to the simulated data obtained from $g_n(\mathbf{u})$ in (5). The results for $\hat{S}_0$ and $\hat{\theta}$ are shown in Figs. 1 and 2, respectively. As can be seen, for SNR above 13 dB the proposed method is statistically efficient since it achieves the CRB. Moreover, for this specific example, since the performance of the LM algorithms are dependent on the initial guess, LORE-GN has better performance than cLM at lower SNR. As expected, using only LORE gives a higher rMSE.

The main reason why LM performs poorly, even at high SNR, is that it sometime converges to a optimum with negative $\hat{a}$, which leads to a shifted $\hat{\theta}$ and rotated $\hat{S}_0$ as mentioned earlier. However, due to the noise and the small value of the true b, the optimum is achieved at a *positive* $\hat{b}$, which means that the post-processing from Eq. (18) cannot correct for this. The problem is not as severe for GN, which has a good enough start value and always converges to the correct optimum with respect to θ, for high SNR. It should be noted that cLM does not find an optimum for any $\hat{b} \geq 0$ when the unconstrained LM finds a $\hat{b} < 0$. The cLM solution ends up on the border of the constraint set. This will effectively decrease the rMSE of the estimate in a rather synthetic manner, since the actual fit of the model might be poor.

A comparison of algorithm complexity in terms of computation time was also performed. The proposed algorithm is 8 times faster than cLM at 15 dB, which has similar performance in this example. This comparison inevitably depends on the implementation but still illustrates the reduction in computation time possible by using our application-specific method. Note that because of the pixel-wise computations the algorithm can easily be parallelized on multi-core computers to further decrease computation time if needed.

4.2 *In Vivo* Data

The dataset used in this example corresponds to the MRI scan of a human brain using the acquisition parameters $TR = 31.2$ ms, $TE = 15.6$ ms and $\alpha = 90^\circ$. Figure 3 shows the magnitude of the data used ($N = 4$), including banding artifacts (some of them indicated by the arrows). The SNR of the data was estimated by measuring the average signal power over the brain and comparing with the variance in the background, which gave an SNR of approximately 13 dB. Finding the region with no tissue is done by thresholding the magnitude image. This also provides a mask which is used to exclude pixels that cannot be modeled. The LORE-GN algorithm was executed on all unmasked pixels. The magnitude of $\hat{S}_0$ is shown in Fig. 4. The magnetization including coil sensitivity can be explicitly obtained from $\hat{S}_0$ by using the estimates $\hat{a}$ and $\hat{b}$, however, the visualization is almost identical in this case. The important part is that $\hat{S}_0$ is independent of θ. As a comparison, the results of the SoS and MI methods are shown in Figs. 5(a) and 5(b), respectively. As can be seen, the proposed algorithm gives a uniform intensity of the magnetization, with no banding artifacts. In the competing images based on SoS and MI, weak banding can still be seen (indicated by the arrows). The estimated off-resonance map ($\hat{f}_{OR}$) is shown in Fig. 6(a) (note that the reference point is arbitrary). The phase was unwrapped using a quality guided path following phase unwrapping algorithm [9]. Phase unwrapping is essential to determine the linear shifts of the resonance frequency since the phase θ can wrap multiple times over an image. Also note that the unwrapped θ values corresponding to Fig. 6(a) are spread in the interval $[0,\ 2\pi]$, which underlines the importance of a good adaptive initial estimate. Any fixed start guess of θ will be off by π for some pixels. By computing the phase of S_0, information about the coil sensitivity K can be obtained since M is purely imaginary (see (2)), this is shown in Fig. 6(b). The runtime for the full algorithm was about 20 s for 6458 pixels on a single 3 GHz core.

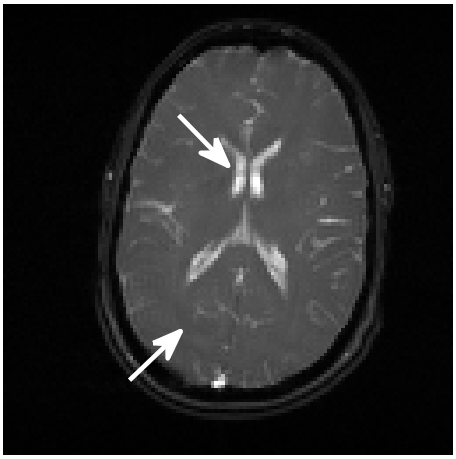

(a)

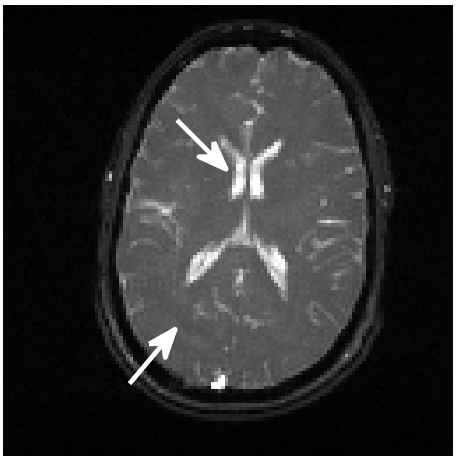

(b)

Figure 5: Results of the (a) SoS and (b) MI methods applied to the images in Fig. 3, still showing some weak banding (indicated by the arrows).

5. CONCLUDING DISCUSSION

A good initial guess is of great importance since there can be multiple local optima in the NLS criterion. Using a fixed (non pixel adaptive) initial value for an iterative NLS minimization can make the algorithm converge to suboptimal solutions, even at high SNR, since the true parameters can vary greatly over an image. This problem is solved by LORE given high enough SNR. The suggested two-step method LORE-GN is fast and performs well as compared to competing methods. Applying the algorithm to *in vivo* data gives a uniform intensity where the banding artifacts are successfully removed, while also providing estimates of the remaining model parameters, such as the off-resonance frequency.

6. ACKNOWLEDGMENT

The authors thank Dr. M. Lustig for providing the *in vivo* data. This work was supported in part by Swedish Foundation for International Cooperation in Research and Higher Education (STINT), and the European Research Council (ERC, agreement numbers 228044 and 247035).

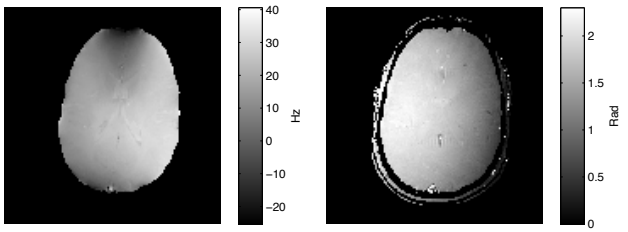

(a) (b)

Figure 6: a) Estimated off-resonance map ($\hat{f}_{OR}$), and b) phase of $\hat{S}_0$ ($\angle\hat{S}_0$) giving information about the coil sensitivity K.

A. THE CRAMÉR-RAO LOWER BOUND (CRB)

The Fisher information matrix under the assumption of circularly Gaussian-distributed, zero-mean, white complex noise of variance σ^2 is given by the Slepian-Bangs formula [6]:

$$\mathbf{I}(\mathbf{u}) = \frac{2}{\sigma^2}\sum_{n=1}^{N}\Re\mathfrak{e}\left\{\left(\frac{\partial g_n(\mathbf{u})}{\partial \mathbf{u}}\right)\left(\frac{\partial g_n(\mathbf{u})}{\partial \mathbf{u}}\right)^*\right\}, \qquad (25)$$

where * denotes the conjugate transpose. The CRB is given by the inverse of the Fisher information matrix $\mathbf{I}^{-1}(\mathbf{u})$, and the diagonal elements give lower bounds on the variance of the corresponding parameter estimates.

REFERENCES

[1] R. Freeman and H. D. W. Hill, "Phase and intensity anomalies in Fourier transform NMR," *J Magn Reson*, vol. 4, pp. 366–383, 1971.

[2] M. L. Lauzon and R. Frayne, "Analytical characterization of RF phase-cycled balanced steady-state free precession," *Concepts in Magnetic Resonance Part A*, vol. 34A, no. 3, pp. 133–143, 2009.

[3] N. K. Bangerter, B. A. Hargreaves, S. S. Vasanawala, J. M. Pauly, G. E. Gold, and D. G. Nishimura, "Analysis of multiple-acquisition SSFP," *Magn Reson Med*, vol. 51, no. 5, pp. 1038–47, 2004.

[4] Q.-S. Xiang and M. N. Hoff, "Simple cross-solution for banding artifact removal in bSSFP imaging," in *Proceedings of the 18th Annual Meeting of ISMRM*, Stockholm, Sweden, 2010.

[5] F. Santini and K. Scheffler, "Reconstruction and frequency mapping with phase-cycled bSSFP," in *Proceedings of the 18th Annual Meeting of ISMRM*, Stockholm, Sweden, 2010.

[6] P. Stoica and R. Moses, *Spectral Analysis of Signals*. Upper Saddle River, N.J.: Prentice Hall, 2005.

[7] T. Söderström and P. Stoica, *System Identification*. Prentice Hall International, 1989. [Online]. Available: http://user.it.uu.se/~ps/sysidbook.pdf

[8] S. Boyd and L. Vandenberghe, *Convex Optimization*. New York, NY, USA: Cambridge University Press, 2004. [Online]. Available: http://www.stanford.edu/~boyd/cvxbook/bv_cvxbook.pdf

[9] D. C. Ghiglia and M. D. Pritt, *Two-Dimensional Phase Unwrapping: Theory, Algorithms and Software*. New York, NY, USA: John Wiley & Sons, 1998.